# RSC Advances

## RSC Advances

www.rsc.org/advances

ROYAL SOCIETY
OF CHEMISTRY

www.rsc.org/advances

# Preparation of layered graphitic carbon nitride/montmorillonite nanohybrids for improving thermal stability of sodium alginate nanocomposites

Lu Liu[ab]，Yongqian Shi[bc]，Bin Yu[bc]，Bibo Wang[bc], Xiaming Feng[bc]，Hui Liu[a]，Panyue Wen[bc]，Bihe Yuan[bc], Yuan Hu*[bc]and Qilong Tai*[bc]

[a]Nano Science and Technology Institute，University of Science and Technology of China, 166 Ren'ai Road, Suzhou, Jiangsu 215123, P.R. China

[b]State Key Laboratory of Fire Science, University of Science and Technology of China, 96 Jinzhai Road, Hefei, Anhui 230026, P.R. China. Email：yuanhu@ustc.edu.cn; Tel:86-551-3601664;Fax:86-551-3601664

[c]USTC-CityU Joint Advanced Research Centre, Suzhou Key Laboratory of Urban Public Safety, Suzhou Institute for Advanced Study, University of Science and Technology of China, 166 Ren'ai Road, Suzhou, Jiangsu 215123, P.R. China. E-mail: qltai@ustc.edu.cn; Fax: +86-512-/87181516; Tel: +86-512-/87161296

**Abstract**

Graphitic carbon nitride (g-$C_3N_4$) / montmorillonite (Na-MMT) nanohybrids were successfully fabricated by a facile mixing strategy and then introduced into sodium alginate host to prepare nanocomposites with different loading levels using a casting technique. The introduction of 4.0 wt% nanohybrids led to the maximal improvement by ca. 149 °C in thermal stability. The improvement of the thermal stability was due to the reason that the mutual intercalation weakened the interlayered interaction of g-$C_3N_4$ nanosheets or Na-MMT sheets and enhanced the physical barrier effect that retarded the permeation of heat and the escape of volatile products. This work may provide an approach for exploiting g-$C_3N_4$ based materials.

*Keywords:* Carbon materials; Multilayer structure; Nanocomposites; Thermal properties; Interfaces.

## 1. Introduction

Graphitic-like carbon nitride (g-$C_3N_4$), with stacked two-dimensional structure, has attracted considerable attention due to its excellent performances[1]. The g-$C_3N_4$ and its various modifications have been widely studied[2,3]. Our group reported that sodium

alginate (SA)/g-C$_3$N$_4$ nanocomposites exhibited a remarkable increase of 118.2 °C in the half thermal degradation temperature at 6.0 wt% loadings[4]. However, the higher loadings are limited due to presence of severe aggregation. It is necessary to improve the loading levels of nanohybrids in polymer matrix. Prior reports about graphene based nanohybrids indicated that synergistic dispersion effect is existent in graphene and its synergists[5,6]. Moreover, scarcely any previous work on g-C$_3$N$_4$ based nanohybrids applied to polymer nanocomposites has been reported.

As a typical two-dimensional layered material, montmorillonite (MMT) and its derivatives have been widely utilized to prepare the polymer nanocomposites. Epoxy / OMMT nanocomposites showed an increase of 30 °C in 10 wt% mass loss at 6 phr loading versus pure epoxy matrix[7]. More than 100% improvement of tensile strength has been reported for 12 phr addition of Cloisite Na$^+$ in rubber[8]. Recently, clay-based nanocomposites have received increasing scientific interest because of its highly desirable qualities including high modulus, significant strength and toughness as well as flame retardancy and low oxygen transmission rate[9]. Given the results above, it is expected that combination of g-C$_3$N$_4$ and MMT could contribute to properties improvement of SA nanocomposites. The aim of our present work was to improve the thermal stability of SA nanocomposites.

## 2. Experimental section

The bulk g-C$_3$N$_4$ was conducted by a procedure similar to that described in prior report[10]. Nanohybrids and SA nanocomposites were synthesized by a facile mixing approach. Na-MMT suspension was vigorously stirred for 3 d at room temperature and then mixed with protonated g-C$_3$N$_4$ under ultrasonic agitation. The as-synthesized nanohybrids labeled as CM (x/y) revealing a weight ratio of g-C$_3$N$_4$ to Na-MMT with x/y (x+y=100), were treated by filtering-washing to get a homogenous distribution. According to the TGA data under air and nitrogen conditions, CM (10/90) shows the best thermal stability and highest char residues among all the nanohybrids (Figure 1S). The mixture of alginate solution and CM (10/90) suspension was agitated for 30 min under ultrasonication. Each solution was degassed and thrown onto flat dish (10×20 cm$^2$) followed by left undisturbed at 40 $^o$C to prepare nanocomposites. These nanocomposites were peeled off from the dish and denoted as SA-0.5, SA-1.0, SA-2.0, SA-4.0 and SA-6.0, corresponding to SA nanocomposites with content of 0.5, 1.0, 2.0, 4.0 and 6.0

wt% nanohybrids, respectively. The schematic representation for the formation of nanocomposites is illustrated in Figure 1a. For comparison, the identical strategy was used to obtain SA-C-4.0 and SA-M-4.0 corresponding to SA nanocomposites with 4.0 wt% g-$C_3N_4$ and Na-MMT, respectively.

X-rays diffraction (XRD) patterns were provided by Japan Rigaku Dmax X-ray diffractometer equipped with graphite monochromatized high-intensity Cu-Kα radiation (λ=1.54178 Å). Fourier transform infrared (FT-IR) spectroscopy was conducted by Nicolet 6700 FT-IR spectrophotometer with scanning from 4000 to 400 cm$^{-1}$. Transmission electron microscopy (TEM) was performed by JEOL 2010 with an acceleration voltage of 200 kV. Thermo Gravimetric Analyzer（TGA） curves were provided by Q5000 thermal analyzer (TA Co., USA) heated from 50 to 800 $^{o}$C at 10 $^{o}$C min$^{-1}$ under air with flow rate of 100 ml min$^{-1}$. The morphology of the fracture surface of nanocomposites was investigated by scanning electron microscopy (SEM) (AMRAY1000B, Beijing R&D Center of the Chinese Academy of Sciences, China).

## 3. Results and discussion

Structural phase of as-obtained nanohybrids is identified using XRD. As can be seen in Figure 1b, Na-MMT exhibits a characteristic peak ($d_{001}$) at ca. 7.07° ($2\theta$). The peak at $2\theta = 27.65°$ is assigned to stacking of the conjugated aromatic system for g-$C_3N_4$[11]. The in-plane repeating unit with a period of 0.672 nm is visible at 13.16°. In the case of nanohybrids, the $d_{001}$ is increased from 12.6 to 15.9 Å, indicating the successful intercalation of g-$C_3N_4$ nanosheets into interlayers of Na-MMT. Moreover, the peak at 27.65° is invisible, implying increased interlayer spacing of the g-$C_3N_4$ nanosheets due to intercalation of Na-MMT sheets.

FT-IR is employed to investigate the microstructure of the nanohybrids, as shown in Figure 1c. The peaks at 3000−3500 cm$^{-1}$ are assigned to N−H stretching vibration and hydrogen bonding interactions[12]. The bands at 1000−1800 cm$^{-1}$ are corresponded to the stretching vibration of connected units; the band at ca. 810 cm$^{-1}$ to vibration of the triazine ring; the peak at 1034 cm$^{-1}$ to Si–O stretching vibration for Na-MMT. The nanohybrids exhibit similar bands to those of g-$C_3N_4$ and Na-MMT. It is noting that the peak at 3450 cm$^{-1}$ associated with O−H stretching vibration is broadened and shifted to lower wavenumbers, suggesting the existence of interaction between g-$C_3N_4$ nanosheets and Na-MMT sheets. These results further confirm the mutual intercalation of the two

end members.

The morphology of as-prepared nanohybrids was studied by TEM. Pure g-C$_3$N$_4$ shows a rippled paper-like structure (Figure 1d). Thin nanosheets on the surface of Na-MMT (marked with red arrow) are observed, indicating the presence of g-C$_3$N$_4$ nanosheets for the nanohybrids[13,14].

The XRD traces of the nanocomposites were plotted in Figure 2a. For virgin SA, the broad peak at $2\theta=13.34°$ shows a rather amorphous structure[15]. In the case of nanocomposites, the peak at 26.63° assigns to Na-MMT strengthens with increasing nanohybrids. The structure of SA is not affected by the nanohybrids, indicating that physical interactions primarily occurred in the interface of the materials[16].

Figure 2b depicted the FT-IR spectra of the nanocomposites. For untreated SA, the peak at 3440 cm$^{-1}$ is associated with O−H stretching vibration; the bands at 1611 and 1437 cm$^{-1}$ to symmetric and asymmetric COO$^-$ stretching vibrations; and the peak at 1050 cm$^{-1}$ to the stretching vibration of C−O−C groups[17]. In addition, a shoulder peak at 1710 cm$^{-1}$ is attributed to −COOH group due to the partial hydrolysis of carboxylate salt. These −OH or −COOH groups provide active sites for hydrogen bonding with −NH$_2$, −NH or −OH of CM (10/90). For the nanocomposites, the peak corresponding to −OH groups is shifted to 3420 cm$^{-1}$, suggesting the interaction of SA chains and CM (10/90) nanosheets through hydrogen bonding[18]. However, there is no change at 1710 cm$^{-1}$ with increase of the nanohybrids. As stated in our previous work, the interaction is very weak. Alternatively, the hydrogen bonding may have induced good interfacial adhesion at the interface SA/CM (10/90), and thus resulted in improving thermal stability of the nanocomposites.

SEM was employed to determine the microstructure of the nanocomposites. The smooth surface is observed for pure SA (Figure 3a). In the case of the nanocomposites, excellent dispersion is maintained at loadings as high as 2.0 wt% (Figures 3b, c and d). However, slight agglomeration occurs at the nanohybrids content exceeding 2.0 wt% (Figure 3e and f). The SEM results indicate that good distribution is achieved at high loading levels due to the fact that the mutual intercalation effect weakens the interlayered interaction of g-C$_3$N$_4$ nanosheets or Na-MMT sheets. Further investigation of the dispersion of the nanohybrids in SA host was performed by TEM measurement. From Figure 4, it is evident that the agglomeration is observed from SA-6.0, which is

supported by SEM results.

The thermal stability of the nanocomposites was evaluated by TGA, as can be observed in Figure 5 and Table 1. For neat SA, the degradation terminated at 220 °C is caused by the traces of moisture. $T_{-5}$ (the temperature at 5 wt% mass loss) is visible at 133.1 °C. Degradation of SA containing hydroxyl, carboxyl groups and polymer chains occurs at 200–580 °C[19]. The temperature at half degradation is estimated using $T_{-50}$. Thermal-oxidized degradation of SA backbone is in the range of 580–700 °C. The nanocomposites are marked by high $T_{-5}$. All the nanocomposites exhibit significantly increased $T_{-50}$ rivalled only by pure SA. The thermal stability of SA-4.0 is improved by 149.8 and 31.7 °C, compared with virgin SA and the results of our prior work, respectively[11]. However, the thermal stability of the nanocomposites declines upon the content higher than 4.0 wt%. It is likely that the thermal stability is deteriorated by serious aggregation weakening the physical barrier effect that retards the permeation of heat and the escape of volatile products. To confirm the assumption that layered barrier effect contributes to the improvement in the thermal stability of the materials, g-$C_3N_4$ along with Na-MMT is incorporated into SA matrix to prepare SA-C-mix-M-4.0 for comparison. It is found that SA-4.0 shows the highest thermal stability with respect to the others, indicating that the mutual intercalation is crucial to the barrier effect.

## 4. Conclusions

The CM (10/90) nanohybrids and SA nanocomposites were prepared by the mild mixing strategy and the casting technique, respectively. TGA results indicated that the thermal stability of the nanocomposites was improved significantly, especially, $T_{-50}$ increased by approximately 149.8 °C. Lower than 4.0 wt%, most of CM (10/90) nanosheets were isolated in SA matrix, resulting in improved thermal stability; higher than 4.0 wt%, the aggregation was present in SA matrices leading to decreased thermal stability due to the weakened interaction between SA chains and CM (10/90) nanosheets. The work may contribute to development of g-$C_3N_4$ based hybrids for polymer composites.

## Acknowledgements

## Notes and references

1 X. C. Wang, K. Maeda, A. Thomas, K. Takanabe, G. Xin, J. M. Carlsson, K. Domen and M.Antonietti,*Nat.Mater.*, 2009, **8**, 76-80.

2 Y. Wang, X. C. Wang and M. Antonietti, *Angew. Chem.*, *Int .Edit.*, 2012, **51**, 68-89.

3 K. Myllymaa, S. Myllymaa, H. Korhonen, M. J. Lammi, H. Saarenpaa, M. Suvanto, T. A. Pakkanen, V. Tiitu and R. Lappalainen, *J. Mater. Sci.-Mater. M.*, 2009, **20**, 2337-2347.

4 Y. Q. Shi, S. H. Jiang, K. Q. Zhou, C. L. Bao, B. Yu, X. D. Qian, B. B. Wang, N. N. Hong, P. Y. Wen, Z. Gui, Y. Hu and R. K. K. Yuen, *Acs. Applied Materials & Interfaces*, 2014, **6**, 429-437.

5 Y. Y. Liang, Y. G. Li, H. L. Wang, J. G. Zhou, J. Wang, Tom. Regier and H. J. Dai, *Nat. Mater. ,* 2011, 780-786.

6 Y. X. Xu, H. Bai, G. W. Lu, C. Li and G. Q. Shi, *J. Am. Chem. Soc.*, 2008, **130**, 5856-5857.

7 B. C. Guo, D. M. Ha and C. G. Cai, *Eur. Polym. J.*, 2004, **40**, 1743-1748.

8 N. I. N. Ismail, A. Ansarifar and M. Song, *Polym. Eng. Sci.*, 2013, **53**, 2603-2614.

9 A. D. Liu and L. A. Berglund, *Carbohyd. Polym.*, 2012, **87**, 53-60.

10 Y. Q. Shi, S. H. Jiang, K. Q. Zhou, B. B. Wang, B. A. Wang, Z. Gui, Y. Hu and R. K. K. Yuen, *Rsc. Adv.,* 2014, **4**, 2609-2613.

11 X. C. Wang, K. Maeda, X. F. Chen, K. Takanabe, K. Domen, Y. D. Hou, X. Z. Fu and M. Antonietti, *J. Am.Chem. Soc.*, 2009, **131**, 1680-+.

12 Y. Qiu and L. Gao, Chem. Commun., 2003, 2378–2379.

13 S. M. Paek, J. U. Jang, S. J. Hwang, J. H. Choy, *Jou. of Phy. Che.* 2006, **67**, 1020-1023.

14 T. S. Yu, J. P. Lin, J. F. Xu, T. Chen and S. L. Lin, *Polym.*, 2005, **46**, 5695-5697.

15 S. G. Kim, G. T. Lim, J. Jegal and K. H. Lee, *J. Membrane. Sci.*, 2000, **174**, 1-15.

16 D. L. Han, L. F. Yan, W. F. Chen and W. Li, *Carbohyd. Polym.*, 2011, **83**, 653-658.

17 C. Sartori, D. S. Finch, B. Ralph and K. Gilding, *Polymer.*, 1997, **38**, 43-51.

18 M. Ionita, M. A. Pandele and H. Iovu, *Carbohyd. Polym.*, 2013, **94**, 339-344.

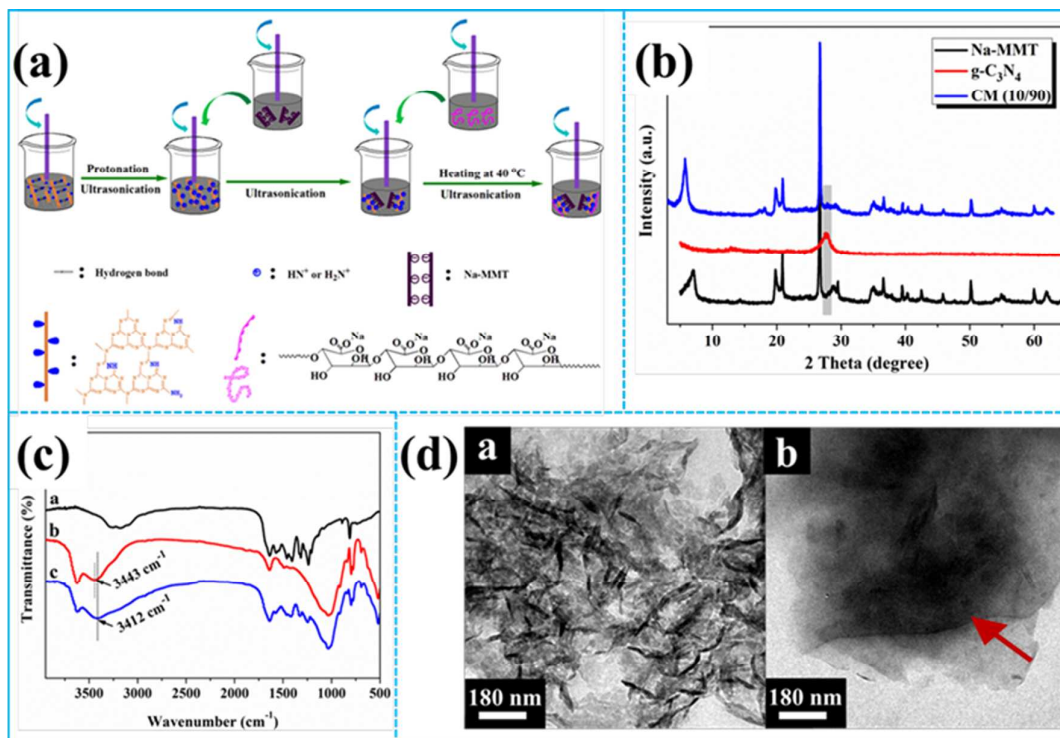19 P. Rani, S. Mishra and G. Sen, *Carbohyd. Polym.*, 2013, **91**, 686-692.

Figure 1. Schematic representation for preparation of CM (10/90) and SA nanocomposites (a), XRD patterns (b) and FT-IR spectra (c) of g-$C_3N_4$ (up), Na-MMT (middle) and CM (10/90) (down), and TEM images (d) of g-$C_3N_4$ (left) and CM (10/90) (right).
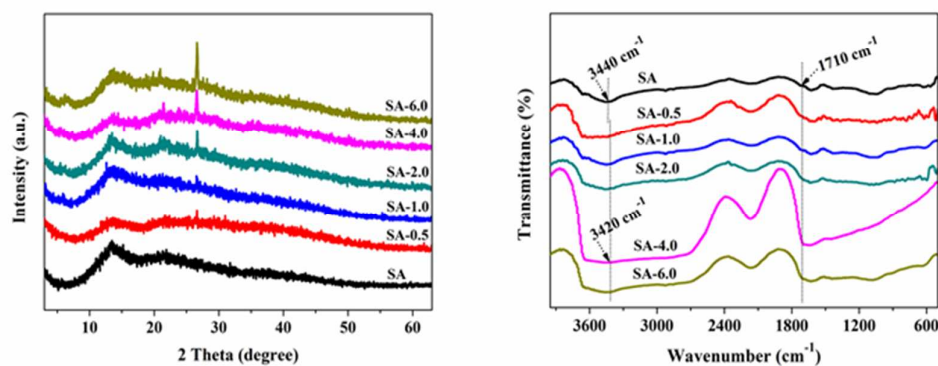


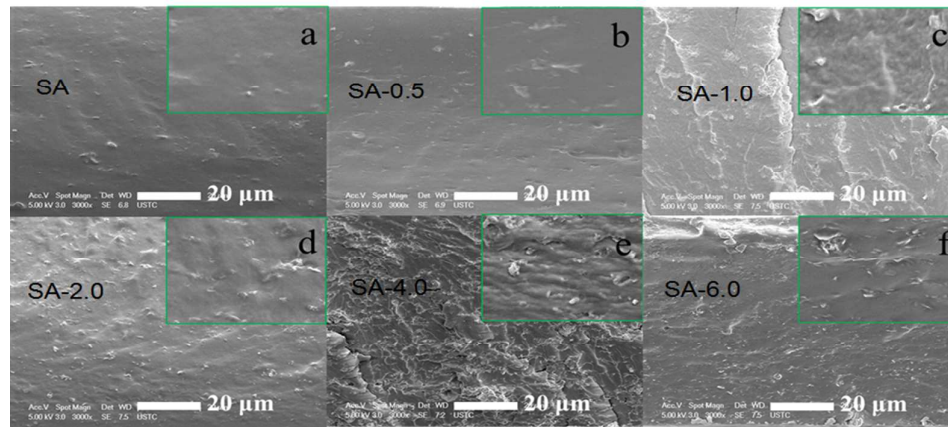Figure 2. XRD patterns (a) and FT-IR spectra (b).

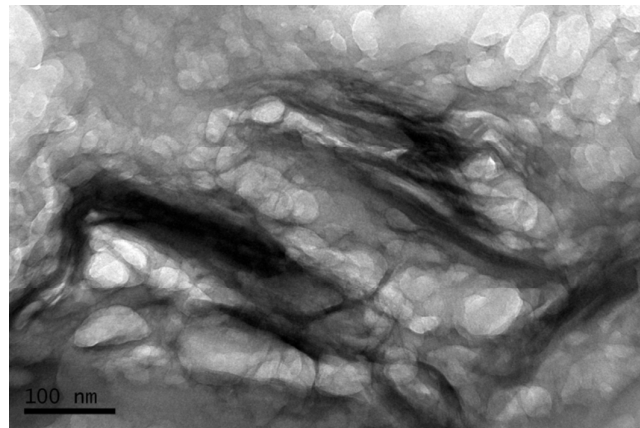Figure 3. SEM images of SA and its nanocomposites.



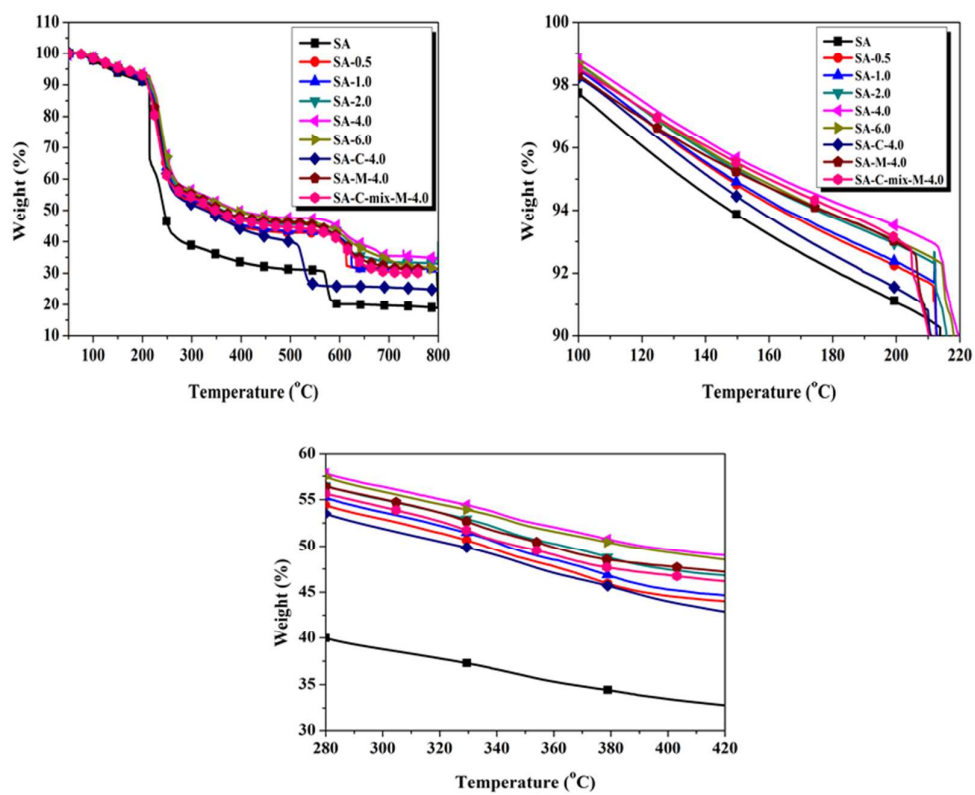Figure 4. TEM ultrathin section image of SA-6.0.

Figure 5. TGA curves of SA and its nanocomposites.

Table 1. The related TGA data of SA and its nanocomposites under air condition.

| Sample | Air | | | |
|---|---|---|---|---|
| | $T_{-5}$ ($^{o}$C) | $T_{-10}$ ($^{o}$C) | $T_{-50}$ ($^{o}$C) | Residues at 800 $^{o}$C (wt %) |
| **SA** | 135.1 | 213.4 | 243.8 | 19.4 |
| **SA-0.5** | 147.2 | 212.7 | 337.4 | 31.4 |
| **SA-1.0** | 147.6 | 212.9 | 344.0 | 31.3 |
| **SA-2.0** | 154.8 | 215.7 | 363.4 | 33.0 |
| **SA-4.0** | 163.7 | 219.6 | 393.6 | 34.7 |
| **SA-6.0** | 156.2 | 218.1 | 387.7 | 31.4 |
| **SA-C-4.0** | 144.4 | 210.7 | 329.0 | 24.7 |
| **SA-M-4.0** | 155.9 | 210.3 | 358.9 | 31.3 |
| **SA-C-mix-M-4.0** | 160.8 | 210.2 | 347.4 | 30.2 |